Article

Journal of
Nanoscience and Nanotechnology
Vol. 19, 7967–7973, 2019
www.aspbs.com/jnn

Preparation of Electrode Modified with Methanobactin Functionalized Gold Nanoparticle and Mimic Superoxide Dismutase Activity

Lin-Lin Chen*, Zhen-Xing Wang, Bo-Xin Dou, Ke Han, Wei Li, and Jia-Ying Xin

Key Laboratory for Food Science and Engineering, Harbin University of Commerce, Harbin 150076, People's Republic of China

Using a mixed self-assembly method, this research utilized modified Mb-functionalized gold nanoparticles (Mb-AuNPs-MPA) on the gold electrode surface to prepare a biosensor which was applied to detect superoxide anion-free electron mediators. Together with the study on the performance of the sensor, the characteristics of modified nanoclusters were investigated by UV-Vis and FTIR and the electrochemical characteristics of the electrode surface were investigated using electrochemical impedance spectroscopy (EIS) and cyclic voltammetry (CV), respectively. It was demonstrated that the charge transfer resistance (Rct) of the modified electrode (Mb-MPA-AuNPs/Au) was 7862 Ω, the exchange current density (i_0) was 32.7 μA/cm^{-2}. And a pair of reversible and symmetrical redox peaks appeared after the coordination of Cu^{2+}, and the electrical signal response of Cu^{2+}/Mb-AuNPs-MPA/Au reached the highest. The superoxide anion generated in the basic DMSO system was determined by CV using the modified electrode Cu^{2+}/Mb-AuNPs-MPA/Au. It was discovered that the superoxide anion had a strong disproportionation effect.

Keywords: Methanobactin, Gold Nanoparticles, Superoxide Dismutase, Modified Electrode.

1. INTRODUCTION

Superoxide dismutase (SOD) plays an important role in protecting cells from the poisoning of oxygen free radicals. SOD can convert superoxide anions ($O_2^{-\cdot}$) in organisms into hydrogen peroxide which can be converted into harmless water by other enzymes, in order to serves the purpose of eliminating oxygen free radicals in the organism and protecting cells. Consequently, SOD is commonly used at clinical treatments for many pathological cases such as cancer, central nervous system damage, radiation damage, and diabetes [1]. Also, SOD performs outstanding effect in the treatment of arterial atherosclerosis, seborrheic dermatitis, and prevention of ischemia and reperfusion injury [2–4]. However, SOD has a large molecular weight [5] and is so easily degraded. In practice, the application of SOD is extremely limited at the present stage. To prepare SOD, disrupted cells need to be isolated and extracted. This is expensive and not easy to preserve. Therefore, the design and synthesis of some novel compounds with high SOD activity can reduce the defects of natural enzymes and has been extensively studied in biochemistry.

The SOD mimetic enzymes obtained by chemical methods are versatile and widely used, but most of them are highly toxic. Thus, it is particularly essential to seek for mimetic enzymes whose natural active substances are ligands. Since most of natural active substances are heavy metal chelating agents, the currently studied ligands are mostly concentrated on small peptides, cyclic peptides, proteins and flavonoids [6–11]. Of the ligands such as peptides and proteins, Methanobactin (Mb) is a copper-binding peptide that appears to function as an agent for copper sequestration and uptake in methanotrophs. In 2003, Choi [12] and others measured the biological activity of Mb, it was found that Mb itself did not possess SOD activity, but the Mb-Cu complex was found to have better SOD activity. In 2008 Choi and others [13] also verified the SOD activity of Mb-Cu.

In addition, gold nanoparticles (AuNPs) have found many applications in bioassays [14–26], the use of gold nanoparticles (AuNPs) can also promote the immobilization of biomolecules on the surface of micro biosensors [27–30] to enlarge the electrical signal on the surface of the electrode. Meanwhile, surface atom coordination of micro biosensors is insufficient and the loss of electrons

*Author to whom correspondence should be addressed.

seriously results in the advantage of strong nanoparticle absorption for biological macromolecules. It is easy to construct a biosensor that can quickly detect $O_2^{-\cdot}$ [31].

In this paper, the bioactive substance Mb was firstly modified on the surface of AuNPs with the aid of the mercaptopropionic acid. The biological activities and structure of Mb were characterized with UV-vis spectroscopy and FTIR spectra. Secondly, in a mixed self-assembly manner, the AuNPs simultaneously modified with the biologically active material Mb and the mercaptopropionic acid were fixed on the surface of the bare gold electrode, coordinating a divalent copper ion on the surface. Finally, CV and EIS were used to characterize the modification process and effect of each modified electrode as well as the detection of the disproportionation ability of $O_2^{-\cdot}$ under basic DMSO conditions.

2. MATERIALS AND METHODS

2.1. Chemicals

Methanobactin (Mb) from the spent medium of *Methylosinus trichosporium* 3011, which was from the Institute of Microbiology and Virology (Kiev, Ukraine), was grown up in a copper-deficient nitrate minimal salt (NMS) medium [32]. Mercaptopropionic acid (MPA) was purchased from Sigma. $HAuCl_4 \cdot 4H_2O$ (the Shanghai No. 1 Reagent Factory) and all other chemicals were analytical grade. All solutions were made up with redistilled water.

2.2. Apparatus and Methods

The UV-vis spectra were recorded with a Shimadzu UV-2550 spectrophotometer (Japan). The FTIR spectra of difference nano-particles were measured using an F-7000 Fourier transform infrared (FTIR) spectrophotometer (HITACHI, Japan).

All electrochemical measurements were performed at a CHI630 electrochemistry work station (Shanghai Chenhua Co., China). The electrochemical cell consisted of a three-electrode system where the modified gold electrode (3 mm in diameter, Shanghai Chenghua, China) was used as the working electrode. The reference electrode was an Ag/AgCl electrode CHI111 (Shanghai Chenhua Co., China). The counter electrode was a platinum wire (99% pure). All glassware used to clean by the freshly aqua regia, rinsed thoroughly in twice-distilled water and dried in air.

2.3. Preparation of Mb Functionalized Gold Nanoparticles

The Mb was prepared and purified according to the references, and the concentration was 0.025 M [33]. The Mb functionalized gold nanoparticles were prepared as follows: Firstly, pure gold nanoparticles were prepared by Frens method. Then, 5 μL of 0.05 M MPA aqueous solution was added into the 2 mL of AuNPs aqueous solution preserved 24 hours at 4 °C to achieve the MPA-AuNPs. Finally, Mb solution was added into the 2 mL of functionalized gold nanoparticles aqueous solution to prepare Mb functionalized gold nanoparticles. All samples were stored in the dark. The prepared nanocomposites were used for all characterization and experiments.

3. RESULTS AND DISCUSSION

3.1. UV-Vis Absorption Spectroscopy (UV-Vis)

As shown in Figure 1, AuNPs gave Soret absorption at 522 nm in their optical absorption spectrum. The wavelength of Mb-AuNPs was 525 nm. However, with the addition of MPA, gold nanoparticles were bathochromic shifted. Also, MPA-AuNPs-Mb absorption changed, this was accompanied by a bathochromic shift of the 525 nm maxima to 690 nm. At the same time the absorption peaks were also decreased. The UV-visible absorption spectrum changed with the addition of MPA. The absorption wavelength of MPA-AuNPs-Mb bathochromic shifted from 530 nm to 534 nm, and the absorption peak also decreased, due to the occurrence of a bathochromic shift coordination of metal ligand (AuNPs) with sulfydryl or carboxyl groups in Mb and MPA charged transfer transitions.

3.2. FTIR Spectra

The binding of biological groups to the gold surface was determined using FTIR as illustrated in Figure 2(a). The marker bands of oxazolone and imidazolone framework were found and these were the characteristic peaks of Mb. As shown in Figure 2(b), the IR spectrum corresponding to Mb-AuNPs also revealed the characteristic absorption peak of Mb showing that Mb molecules were attached to the surface of AuNPs. Among them, the stretching vibration of –S–S– was at 439 cm^{-1}. After adding AuNPs, the stretching vibration of –S–S– at 439 cm^{-1} was significantly reduced [34]. This presented that Mb was coupled with gold nanoparticles through disulfide

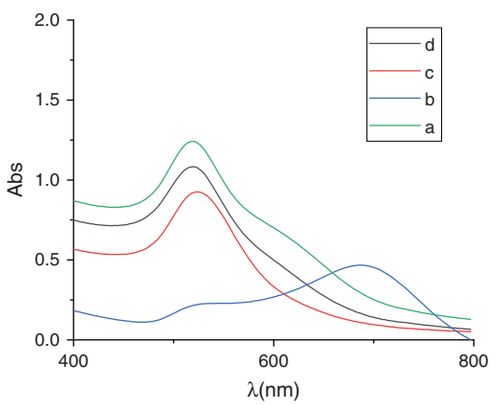

Figure 1. The UV-spectra of pure gold nanoparticles (a), Mb-AuNPs (b), MPA-AuNPs (c), and Mb functionalized gold nanoparticles (d).

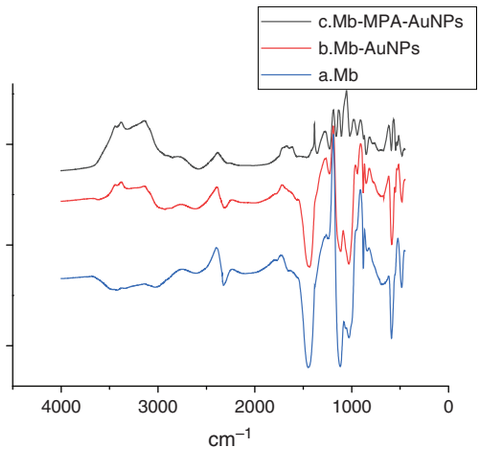

Figure 2. FTIR spectra of Mb (a), Mb-AuNPs (b), and Mb-MPA-AuNPs (c).

bonds, forming a coordination bond between sulfur and gold.

Comparing Mb-AuNPs with MPA-AuNPs-Mb, it was found they not only had the biological activity of Mb, but also AuNPs provided more active sites for Mb, making Mb possess a better spatial conformation and activity.

3.3. Electrochemical Impedance Spectroscopy (EIS)

EIS is an effective method to obtain the electrode reaction parameters such as the hetero charge transfer resistance and the exchange current density [35, 36]. In the test, the surface resistances of the electrodes during the modification of the electrode were determined by the EIS. The EIS curves were shown in Figure 3. Nyquist curve of the bare gold electrode, which was a very small semicircle domain, was shown in Figure 3(a). Impedance arc was not observed at high frequencies, this means that the reaction at the gold electrode was controlled by diffusion. After the MPA was

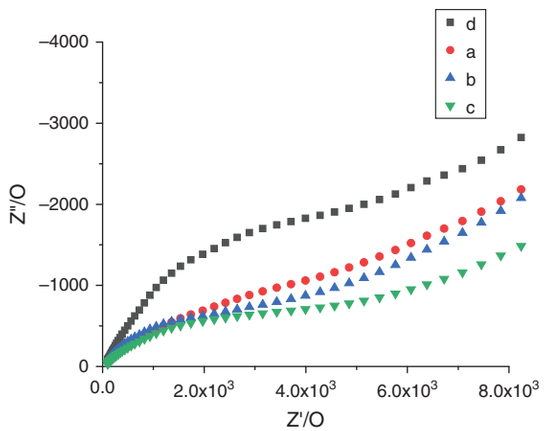

Figure 3. The electrochemical impedance spectroscopies of (a) bare gold electrode, (b) Mb modified gold electrode, (c) Mb-AuNPs modified gold electrode, and (d) MPA-AuNPs-Mb modified gold electrode.

assembled, the impedance curve appeared in the high frequency part of the curve, it implied that the monolayer had an inhibitory effect on the electron transfer of the electrode surface. However, the prepared Mb functionalized gold nanoparticles were modified to a bare gold electrode by self-assembly, the impedance arc radius of the high frequency part was significantly increased, indicating that the barrier of the film to the electron transport was enhanced. Therefore, the reaction at the high frequency part of the electrode was controlled by the kinetics.

As was shown, the charge transfer resistance (R_{ct}) of all electrodes could be calculated. Because of R_{ct} of the bare gold electrode was so small, the semicircle was almost invisible in the AC impedance spectrum [37]. By the formula $R_{CT} = RT/(Fi_0)$ and $i_0 = nFAk_0C_o^{(1-T)}C_r^T$. C_o and C_r are the concentrations of $Fe(CN)_6^{3-}$ and $Fe(CN)_4^{-6}$ respectively. A, R, T, and F are the electrochemical area, gas constant, temperature, and Faraday constant. The electron transfer coefficient and transfer rate of the bare gold electrode are taken as 1 and 0.026 cm/s. The R_{ct} of the bare gold electrode was 740 Ω. After the modification of Mb on the bare gold electrode substrate, the R_{ct} changed dramatically to 1948 Ω, which demonstrated that the presence of the bare gold electrode and Mb could greatly reduce the conductivity of the electrode and inhibited the electron transfer between the electrolyte and the electrode interface. When Mb functionalized gold nanoparticle was immobilized on the electrode, the R_{ct} showed a slight increase to 7862 Ω, indicating that the immobilization of methanobactin functionalized gold nanoparticle would cause an insulating effect on the electrode and increased the Rct. The amount of i_0 quantitatively reflected the magnitude of the out-of-phase charge transfer rate. Various electrodes were 347.1, 131.9, 60.7 and 32.7 $\mu A/cm^{-2}$, respectively [38].

3.4. Cyclic Voltammograms (CV)

In order to find out whether Mb functionalized gold nanoparticle was immobilized on the surface of the bare gold electrode films and formed stable and orderly self-assembled films, $Fe(CN)_6^{3-}/Fe(CN)_6^{4-}$ as a redox probe was utilized. The CV showed the same results as the EIS and implied that the surface of the gold electrode modified with Mb functionalized gold nanoparticles had more materials to hinder electrons transport. Figure 4 showed CVs of different modified electrodes.

As a result, it was found that after the Mb was applied dropwise on the bare gold electrode, the oxidation peak shifted positively, and the reduction peak shifted negatively. The ΔE_p increased by 39.03 mV. When the Mb-AuNPs were modified on the bare gold electrode, the oxidation peaks continued to move forward, the reduction peaks continued to shift negatively, the ΔE_p value increased by 34 mV, and the peak current I_p decreased in turn. When the MPA-Mb-AuNPs were also modified on

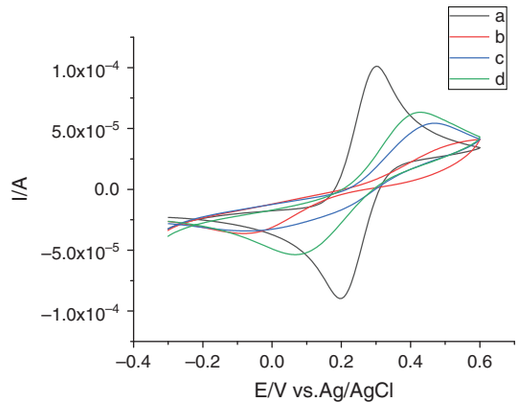

Figure 4. Cyclic voltammograms obtained using 0.1 M KCl solution containing 5.00×10^{-3} M $K_3[Fe(CN)_6]$ and 5.00×10^{-3} M $K_4[Fe(CN)_6]$ at a 3 mm diameter gold electrode modified by (a) bare gold electrode, (b) Mb modified gold electrode, (c) Mb-AuNPs modified gold electrode, and (d) MPA-AuNPs-Mb modified electrode at a scan rate of 100 $mV \cdot s^{-1}$, respectively.

the bare gold electrode, the ΔE_p value was again increased by 78.26 mV, while the peak current I_p was also decreased, which might be due to the barrier effect of the monolayer on the electron transfer of the electrode/solution interface, and the reversibility of the electrode became worse and worse [39]. This showed that the modified electrode formed a of molecular layer with considerable coverage on the surface of the gold electrode and bonded the nanocluster to the surface of the electrode.

3.5. Superoxide Detection

3.5.1. Cyclic Voltammograms of Mb-Cu Modified Electrodes

Mb and Mb-Cu exhibited a range of reduction potentials. Figure 5 showed that the redox capacities of different modified electrodes before and after coordination with Cu^{2+} were tested. In the reaction system, the bare gold electrode did not generate a redox peak in the CV test. However, when Mb was modified to gold electrode by self-assembly, weak redox signal appeared on the surface of all kinds of electrodes. But the Mb-Cu complex showed stronger reduction than that of Mb. After the coordination of Cu^{2+}, a pair of reversible and symmetrical oxidation and reduction peaks appeared for each modified electrode under CV test. After the coordination of Cu^{2+}, the reduction potential and oxidation peak potential of the Mb/Au electrode were 0.213 and 0.385 V, the reduction potential and oxidation peak potential of the Mb-AuNPs/Au electrode were 0.174 and 0.333 V, the potentials at the appearance of the reduction and oxidation peaks of the Au modified electrode were 0.172 and 0.311 V [40].

3.5.2. Determination of Disproportionation for $O_2^{-\cdot}$ by Modified Electrode

From the analysis of Section 3.5.1, it can be seen that no matter which compound was modified on the bare

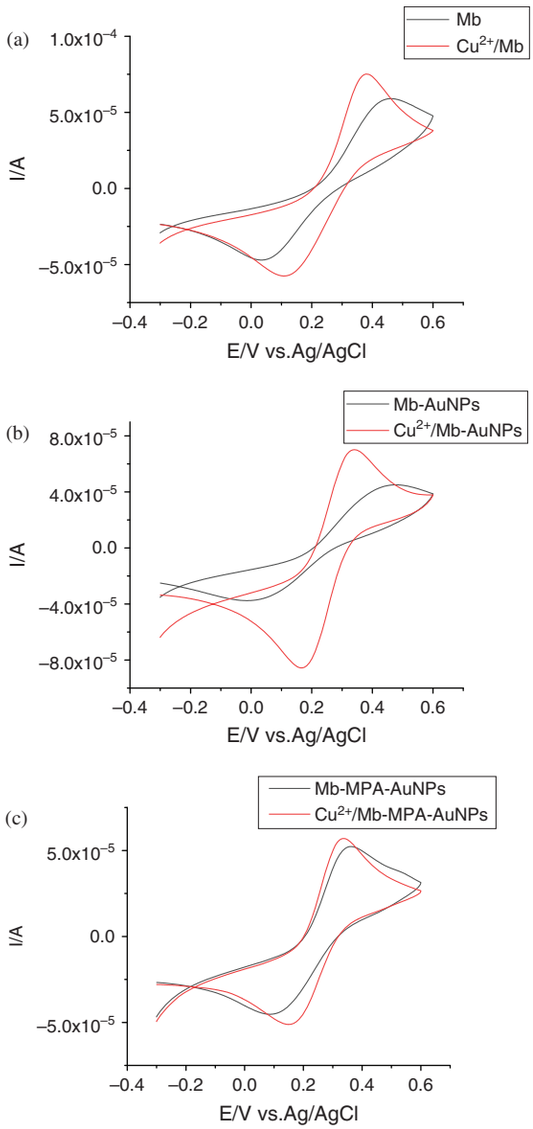

Figure 5. Cyclic voltammograms obtained from 0.1 M KCl solution containing 5.00×10^{-3} M $K_3[Fe(CN)_6]$ and 5.00×10^{-3} M $K_4[Fe(CN)_6]$ at a 3 mm diameter gold electrode modified by Mb (a), Mb-AuNPs (b), and Mb-AuNPs-MPA (c) before and after coordination with copper ion, at a scan rate of 50 $mV \cdot s^{-1}$, respectively.

gold electrode, the redox peak current of the coordination Cu^{2+} was higher than that of the uncoordinated Cu^{2+}. However, in those modified electrodes, the current corresponding to the oxidation and reduction potentials of the modified electrode of MPA-AuNPs-Mb/Au coordinated with Cu^{2+} was the largest, Therefore, it was used as a modified electrode to determine the disproportionation of $O_2^{-\cdot}$.

The CVs before and after the addition of NaOH to the Cu^{2+}/MPA-AuNPs-Mb/Au modified electrode in the DMSO reaction system (Fig. 6) were compared [41]. It can be seen that the corresponding oxidation-reduction peak

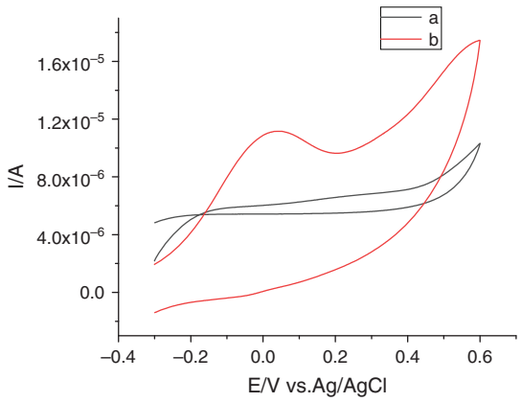

Figure 6. Cyclic voltammograms of Cu^{2+} coordination modified electrode (MPA-AuNPs-Mb/Au) in DMSO (5 mL total volume) without NaOH (a) and with addition of 5 M NaOH solution (5 μL) (b) at scan rate 100 mV/s.

current of the modified electrode after the addition of NaOH was relatively increased with the addition of NaOH, indicating that the Cu^{2+}/MPA-AuNPs-Mb/Au modified electrode had certain degree of disproportionation to $O_2^{-\cdot}$. The increase in oxidation peak and reduction peak current in the graph was due to the redox reaction of the $O_2^{-\cdot}$.

On the surface of gold electrode, due to the oxidation of $O_2^{-\cdot}$ by Cu^{2+}/MPA-AuNPs-Mb, the electrode surface part of the Cu^{2+}/MPA-AuNPs-Mb was converted to Cu^{+}/MPA-AuNPs-Mb (Fig. 7). In other words, when $O_2^{-\cdot}$ was present, the concentration of Cu^{+}/MPA-AuNPs-Mb on the surface of the electrode was greater than that no $O_2^{-\cdot}$. On the CV, the anode peak current increased when the electrode underwent electrochemical oxidation. Moreover, Cu^{+}/MPA-AuNPs-Mb also had a certain reduction effect on $O_2^{-\cdot}$, the Cu^{2+}/MPA-AuNPs-Mb was converted to Cu^{+}/MPA-AuNPs-Mb, increased the concentration of Cu^{2+}/MPA-AuNPs-Mb on the gold electrode surface. Therefore, when the electrode underwent electrochemical reduction, the peak current of the cathode also increased [42].

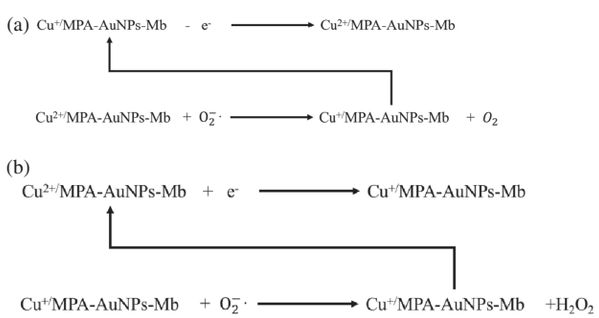

Figure 7. Redox peak current increase schematic, oxidation peak current increase schematic (a) reduction peak current increase schematic (b)

4. CONCLUSIONS

Through MPA and AuNPs, we prepared functionalized gold nanoparticles MPA-AuNPs-Mb that retained the biological activity of Mb. The structure was characterized by UV-Vis and FTIR spectra. The nanoparticles significantly improved the agglomeration of gold nanoparticles. Using Mb functionalized gold nanoparticle as the basic element, it was modified to a bare gold electrode surface by a hybrid self-assembly method to form a dense and ordered three-dimensional self-assembled membrane structure. After coordination of divalent Cu^{2+}, the redox capacity of various materials modified with Mb was significantly increased, and the response of Cu^{2+}/MPA-AuNPs-Mb/Au modified electrode was the highest. The $O_2^{-\cdot}$ produced in the basic DMSO system was determined by CV using the Cu^{2+}/MPA-AuNPs-Mb/Au modified electrode. The results showed that the Cu^{2+}/MPA-AuNPs-Mb/Au modified electrode had certain degree of disproportionation to $O_2^{-\cdot}$.

Acknowledgment: The authors thank the Scientific research project in school-level of Harbin University of Commerce (18XN079), Harbin Applied Technology Research and Development Project (2014RFQXJ115), 2017 Graduate Innovation Research Project of Harbin University of Commerce (YJSCX2017-461HSD), Youth Innovative Talents Program Project of Harbin University of Commerce (17XN021) and National natural science foundation of China (21573055) for support, and the Laboratory of Biocatalysis, Food engineering college, Harbin Commerce University of China are gratefully acknowledged.

References and Notes

1. Batinic-Haberle, I., Rajic, Z., Tovmasyan, A., Reboucas, J.S., Ye, X., Leong, K.W., Dewhirst, M.W., Vujaskovic, Z., Benov, L. and Spasojevic, I., **2011**. Diverse functions of cationic Mn(III) N-substituted pyridylporphyrins, recognized as SOD mimics. *Free Radic. Biol. Med., 51*(5), pp.1035–53.
2. Dong Hoon, K. and Sang Won, K., **2013**. Targeting cellular antioxidant enzymes for treating atherosclerotic vascular disease. *Biomol. Ther. (Seoul), 21*(2), pp.89–96.
3. Ozturk, P., Arican, O., Belge Kurutas, E., Karakas, T. and Kabakci, B., **2013**. Oxidative stress in patients with scalp seborrheic dermatitis. *Acta Dermatovenerol. Croat., 21*(2), pp.80–5.
4. Karahalil, B., Kesimci, E., Emerce, E., Gumus, T. and Kanbak, O., **2011**. The impact of OGG1, MTH1 and MnSOD gene polymorphisms on 8-hydroxy-2′-deoxyguanosine and cellular superoxide dismutase activity in myocardial ischemia-reperfusion. *Molecular Biology Reports, 38*(4), pp.2427–35.
5. Wang, Y., Yang, Z.Y. and Wang, B.D., **2005**. Synthesis, characterization and anti-oxidative activity of Cobalt(II), Nickel(II) and Iron(II) Schiff base complexes. *Transition Metal Chemistry, 30*(7), pp.879–883.
6. Li, C., Yang, Z., She, M.X., Yin, W.T., Li, J.L., Zhao, G.F. and Shi, Z., **2011**. Recent progress in superoxide dismutase mimics. *Chemical Journal of Chinese Universities, 32*(9), pp.2046–2061.
7. Güngör, S.A., Köse, M., Tümer, F. and Tümer, M., **2016**. Photoluminescence, electrochemical, SOD activity and selective chemosensor properties of novel asymmetric porphyrin-Schiff base compounds. *Dyes and Pigments, 130*(7), pp.37–53.

8. Tovmasyan, A., Bueno-Janice, J.C., Spasojevic, I. and Batinic-Haberle, I., **2017**. 33-Novel fluorinated Mn porphyrin as a powerful SOD mimic and catalyst for ascorbate-coupled anticancer therapy. *Free Radical Biology and Medicine, 112*(S1), pp.36–37.

9. Yuan, Z.L., Wu, Q., Yang X.B., Hu, Q.H., Zhong, Y.K., Zhou, X.M. and Zhang, M.Q., **2011**. Synthesis and activity study of SOD novel water-soluble Schiff base macrocycic Mn (II) compounds. *Chinese Journal of Synthetic Chemistry, 19*(4), pp.446–449.

10. Joseph, J. and Ayisha Bibin Rani, G., **2017**. Metal based SOD mimetic therapeutic agents: Synthesis, characterization and biochemical studies of metal complexes. *Arabian Journal of Chemistry, 10*(S2), pp.S1963–S1972.

11. Zhou, Y.H., Liu, X.W., Chen, L.Q., Wang, S.Q. and Cheng, Y., **2016**. Synthesis, structure and superoxide dismutase-like activity of two mixed-ligand Cu(II) complexes with N,N′-bis(2-pyridylmethyl)amantadine. *Polyhedron, 117*(7), pp.788–794.

12. Choi, D.W., Kunz, R.C., Boyd, E.S., Semrau, J.D., Antholine, W.E., Han, J.I., Zahn, J.A., Boyd, J.M., de la Mora, A.M. and DiSpirito, A.A., **2003**. The membrane-associated methane monooxygenase (pMMO) and pMMO-NADH: Quinone oxidoreductase complex from *Methylococcus capsulatus* bath. *Journal of Bacteriology, 185*(19), pp.5755–5764.

13. Choi, D.W., Semrau, J.D., Antholine, W.E., Hartsel, S.C., Anderson, R.C., Carey, J.N., Dreis, A.M., Kenseth, E.M., Renstrom, J.M., Scardino, L.L., Van Gorden, G.S., Volkert, A.A., Wingad, A.D., Yanzer, P.J., McEllistrem, M.T., de la Mora, A.M. and DiSpirito, A.A., **2008**. Oxidase, superoxide dismutase, and hydrogen peroxide reductase activities of methanobactin from types I and II methanotrophs. *Journal of Inorganic Biochemistry, 102*(8), pp.1571–1580.

14. Zhang, L., Xia, K., Bai, Y.-Y., Lu, Z., Tang, Y., Deng, Y., Chen, J., Qian, W., Shen, H., Zhang, Z., Ju, S. and He, N., **2014**. Synthesis of gold nanorods and their functionalization with bovine serum albumin for optical hyperthermia. *Journal of Biomedical Nanotechnology, 10*(8), pp.1440–1449.

15. Lai, Y., Zhang, C., Deng, Y., Yang, G., Li, S., Tang, C. and He, N., **2019**. A novel α-fetoprotein-MIP immunosensor based on AuNPs/PTh modified glass carbon electrode. *Chinese Chemical Letters, 30*(1), pp.160–162.

16. Li, T., Yi, H., Liu, Y., Wang, Z., Liu, S., He, N., Liu, H. and. Deng, Y., **2018**. One-step synthesis of DNA templated water-soluble Au-Ag bimetallic nanoclusters for ratiometric fluorescence detection of DNA. *Journal of Biomedical Nanotechnology, 14*(1), pp.150–160.

17. Zhang C., Huang, Y., Fang, Y., Liao, P., Wu, Y., Chen, H., Chen, Z., Deng, Y, Li, S., Liu and He, N., **2019**. The liquid level detection system based on pressure sensor. *Journal of Nanoscience and Nanotechnology, 19*(4), pp.2049–2053.

18. Zhang, L., Xia, K., Lu, Z., Li, G., Chen, J., Deng, Y., Li, S., Zhou, F. and He, N., **2014**. Efficient and facile synthesis of gold nanorods with finely tunable plasmonic peaks from visible to near-IR range. *Chemistry of Materials, 26*(5), pp.1794–1798.

19. Liao, P., Fang, Y., Chen, H., Wu, Y., Deng, Y., Chen, Z., He, N., Liu, H. and Li, S., **2019**. Quickanalysis: A software designed and developed for a portable on-site pathogen detection system. *Journal of Nanoscience and Nanotechnology, 19*(4), pp.2054–2059.

20. Yang, H., Liu, M., Jiang, H., Zeng, Y., Jin, L., Luan, T., Deng, Y., He, N., Zhang, G. and Zeng, X., **2017**. Copy number variation analysis based on gold magnetic nanoparticles and fluorescence multiplex ligation-dependent probe amplification. *Journal of Biomedical Nanotechnology, 13*(6), pp.655–664.

21. Chen, Z., Fang, C., Wang, H. and He, J., **2009**. Disposable glucose test strip for whole blood with integrated sensing/diffusion-limiting layer. *Electrochimica Acta, 55*(2), pp.544–550.

22. Ahmad, R., Fu, J., He, N. and Li, S., **2016**. Advanced gold nanomaterials for photothermal therapy of cancer. *Journal of Nanoscience and Nanotechnology, 16*(1), pp.67–80.

23. Cao, L.L., Fang, C., Zeng, R.S., Zhao, X.J., Jiang, Y.R. and Chen, Z.C., **2017**. Paper-based microfluidic devices for electrochemical immunofiltration analysis of human chorionic gonadotropin. *Biosensors and Bioelectronics, 92*(6), pp.87–94.

24. Liu, Y., Deng, Y., Li, T., Chen, Z., Chen, H., Li, S. and Liu, H., **2018**. Aptamer-based electrochemical biosensor for mercury ions detection using AuNPs-modified glass carbon electrode. *Journal of Biomedical Nanotechnology, 14*(12), pp.2156–2161.

25. Huang, Y., Xia, K., He, N., Lu, Z., Zhang, L., Deng, Y. and Nie, L., **2015**. Size-tunable synthesis of gold nanorods using pyrogallol as a reducing agent. *Science China-Chemistry, 5*(11), pp.1759–1765.

26. Mao, L., Lu, Z., He, N., Zhang, L., Deng, Y. and Duan, D., **2017**. A new method for improving the accuracy of miRNA detection with $NaYF_4$:Yb,Er upconversion nanoparticles. *Science China-Chemistry, 60*(1), pp.157–162.

27. Liu, Y, Lai, Y.X., Yang, G.J., Tang, C.L., Deng, Y., Li, S. and Wang, Z.L., **2017**. Cd-aptamer electrochemical biosensor based on AuNPs/CS modified glass carbon electrode. *Journal of Biomedical Nanotechnology, 13*(10), pp.1253–1259.

28. Cao, L., Fang, C., Zeng, R., Zhao, X., Zhao, F., Jiang, Y. and Chen, Z., **2017.** A disposable paper-based microfluidic immunosensor based on reduced graphene oxide-tetraethylene pentamine/Au nanocomposite decorated carbon screen-printed electrodes. *Sensors and Acutors B: Chemical, 252*(11), pp.44–54.

29. Lai, Y., Wang, L., Liu, Y., Yang, G., Tang, C., Deng, Y. and Li, S., **2018**. Immunosensors based on nanomaterials for detection of tumor markers. *Journal of Biomedical Nanotechnology, 14*(1), pp.44–65.

30. Lai, Y., Deng, Y., Yang, G., Li, S., Zhang, C. and Liu, X., **2018**. Molecular imprinting polymers electrochemical sensor based on AuNPs/PTh modified GCE for highly sensitive detection of carcinomaembryonic antigen. *Journal of Biomedical Nanotechnology, 14*(10), pp.1688–1694.

31. Dou, B.X. and Xin, J.Y., **2016**. Functional self-assembly gold nanoparticle modified electrodes and application in the field of biosensors with enzyme immobilization. *Journal of Molecular Catalysis (China), 30*(4), pp.391–400.

32. Xin, J.Y., Zhang, Y.X., Dong, J., Zhou, Q.Q., Wang, Y., Zhang, X.D. and Xia, C.G., **2010**. Epoxypropane biosynthesis by whole cell suspension of methanol-growth methylosinus trichosporium IMV 3011. *World Journal of Microbiology and Biotechnology, 26*(4), pp.701–708.

33. Xin, J.Y., Lin, K., Wang, Y. and Xia, C.G., **2014**. Methanobactin-mediated synthesis of gold nanoparticles supported over Al_2O_3 toward an efficient catalyst for glucose oxidation. *International Journal of Molecular Sciences, 15*(12), pp.21603–21620.

34. Li, C.Y., Xin, J.Y., Lin, H.Y., Zhang, Y. and Xia, C.G., **2017**. Study on functionalized gold nanoparticles of methanobactin by copper ion coordination uesd as simulated peroxidase. *Journal of Molecular Catalysis (China), 31*(5), pp.480–485.

35. Nahir, T.M. and Bowden, E.F., **1994**. Impedance spectroscopy of electroinactive thiolate films adsorbed on gold. *Electrochimica Acta, 39*(16), pp.2347–2352.

36. Bandyopadhyay, K., Vijayamohanan, K., Shekhawat, G.S. and Gupta, R.P., **1998**. Impedance analysis of self-assembled naphthalene disulfide monolayer on gold using external redox probes. *Journal of Electroanalytical Chemistry, 447*(1), pp.11–16.

37. Chen, T., Zhang, A.D., Pan, K.H., Mei, F.S. and Liao, Z.R., **2004**. Self assembly of a model compound of superoxide dismutase on gold electrode. *Journal of Central China Normal University (Natural Sciences), 38*(4), pp.455–458.

38. Bandow, N., Gilles, V.S., Freesmeier, B., Semrau, J.D., Krentz, B., Gallagher, W., McEllistrem, M.T., Hartsel, S.C., Choi, D.W., Hargrove, M.S., Heard, T.M., Chesner, L.N., Braunreiter, K.M., Cao, B.V., Gavitt, M.M., Hoopes, J.Z., Johnson, J.M., Polster, E.M., Schoenick, B.D., Umlauf, A.M. and DiSpirito, A.A., **2012**. Spectral and copper binding properties of methanobactin from the facultative methanotroph methylocystis strain SB2. *Journal of Inorganic Biochemistry, 110*(5), pp.72–82.

39. Tang, J., Zhu, X., Niu, X., Liu, T., Zhao, H. and Lan, M., **2015**. Anamperometric superoxide anion radicalbiosensor based on SOD/PtPd-PDARGO modified electrode. *Talanta, 137*(5), pp.18–24.

40. El Ghazouani, A., Baslé, A., Gray, J., Graham, D.W., Firbank, S.J. and Dennison, C., **2012**. Variations in methanobactin structure influences copper utilization by methane-oxidizing bacteria. *Proceedings of the National Academy of Sciences of the United States of America, 109*(22), pp.8400–8404.

41. Chen, S., Lu, Y., Yan, X., Hu, G., Zhu, H. and Xie, H., **1991**. Studies on production of superoxide radical and its interaction with natural medicine. *Journal of Fudan University (Natural Science), 30*(1), pp.31–36.

42. Bi, L., **2006**. Electrochemical study of CdS nanoparticles and superoxide dismutase based on self assembled monolayers. Master's Thesis, Central China Normal University, Hubei, China.

Received: 5 September 2018. Accepted: 5 November 2018.